

SELECTING OPTIMAL NUMERICAL INTEGRATION RULES FOR DOUBLE SURFACE INTEGRALS ON TRIANGULAR DOMAINS

Mario CVETKOVIĆ¹, Dragan POLJAK¹, Ante LOJIĆ KAPETANOVIĆ¹, and Hrvoje DODIG²

¹*FESB, University of Split, Croatia, mcvetkov@fesb.hr, dpoljak@fesb.hr, alojic00@fesb.hr*

²*Faculty of Maritime Studies, University of Split, Croatia, hdodig@fst.hr*

Abstract. This work is on a rather simple and intuitive approach for the selection of optimal quadrature order in terms of lowest number of integration points while retaining the required accuracy. To demonstrate this the Dunavant's symmetrical quadrature rules for triangles are utilized to numerically solve one of the double surface integrals occurring in the numerical solution of integral equation formulations. Examples of several triangle combinations at various radio frequencies are given. The real and imaginary parts of the solution are presented using a P,Q -square in order to illustrate the proposed approach.

Keywords—Numerical integration, Dunavant rules, integral equation formulation, double surface integrals

I. INTRODUCTION

The numerical solution of the integral equation based formulations such as electric field integral equation (EFIE) requires the solution of various double surface integrals. Depending on the distance between the source and the observation points, as well as whether the kernel is regular or singular, the evaluation of such integrals requires different approach. In many situations the integrals can be solved using a numerical quadrature or a combination of numerical and analytical approach.

Choosing the optimal numerical integration order when solving the double surface integrals by purely numerical means is no simple task. If the selected quadrature order, i.e. number of integration points, is too low, the approach could lead to incorrect solution to the integral. On the other hand, selection of higher than necessary quadrature order could lead to needless waste of computational resources in terms of longer computational time without benefit of additional precision. Thus, the approach to select an optimal quadrature order with lowest number of integration points while at the same time retaining required accuracy could be beneficial.

II. METHODOLOGY

This work is based on the frequency domain formulation for the homogeneous lossy dielectric [1]. The electric field integral equation (EFIE) can be obtained using the equivalence theorem for the object surface and the boundary conditions:

$$[-\vec{E}_n^{sca}(\vec{J}, \vec{M})]_{tan} = \begin{cases} [\vec{E}^{inc}]_{tan}, & i = 1 \\ 0, & i = 2 \end{cases} \quad (1)$$

where E^{inc} represents the known incident electric field impinging the scatterer and E^{sca} denotes the field scattered from the object.

The tangential component of the electric field scattered from object surface can be written in terms of the equivalent surface electric and magnetic currents, \vec{J} and \vec{M} , respectively, which can be expanded in terms of a linear combination of basis functions.

In the numerical solution of EFIE [3], to expand the unknown electric current density \vec{J} , usually the RWG functions [4], defined over triangles, are selected as basis functions \vec{f}_n . After testing with \vec{f}_m and integrating over the surface, the following double surface integral could be found:

$$A_{mn} = \iint_S \vec{f}_m(\vec{r}) \cdot \iint_{S'} \vec{f}_n(\vec{r}') G(\vec{r}, \vec{r}') dS' dS \quad (2)$$

where $G(\vec{r}, \vec{r}')$ represents the Green's function for the homogeneous space, and \vec{r} and \vec{r}' denote observation and source points, respectively.

Depending on the distance between source and observation triangles, respectively, particular approach to the solution of (2) is necessary. When observation and source triangles are far enough, numerical integration can be used. The numerical procedure (Gaussian quadrature) carried out in this work is related to evaluation of integral (2) in case of a coplanar source and observation triangles, as illustrated on Fig. 1.

Both surface integrals from (2) can be approximated using a weighted coefficients sum. On a triangular domain, this approximation can be written as:

$$\iint_T f(\alpha, \beta, \gamma) dS \approx A \sum_{i=1}^N w_i(\alpha_i, \beta_i, \gamma_i) f(\alpha_i, \beta_i, \gamma_i) \quad (3)$$

where A denotes the triangle area, $w_i(\alpha_i, \beta_i, \gamma_i)$ are the weighting coefficients normalized with respect to triangle area, while α_i , β_i , and γ_i are local coordinates defined on the unit triangle.

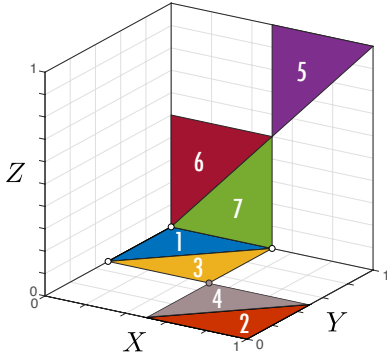


Fig. 1. Unit cube for testing different combinations of source and observation triangles [2].

The numerical solution of (2) is obtained using various integration orders P and Q for source and observation triangles, respectively, with $P = 1, \dots, 20$ and $Q = 1, \dots, 20$, using the location of Gaussian points and the associated weights according to Dunavant's rules [5].

Dunavant's rules are one of the most used integration rules for triangles, and similar to classical Gaussian quadratures, an n -point rule is exact for all polynomials of orders up to $2n - 1$, [6]. These rules are optimal in the sense that for a given rule, the number of utilized nodes is close to or even equal to the smallest possible value [7], a feature that makes them highly efficient in situations when large number of integrals needs to be solved. Additionally, the symmetrical position of the integration nodes with respect to the vertices of the triangles, eliminates the possible variations in the way in which they are assigned [7].

III. RESULTS

Based on the unit cube test, utilized for testing the interaction between source and observation triangles [8], the following results are obtained. The first set of results, related to numerical solution of double surface integral (2) in case of far triangles and near triangles sharing an edge, are shown on Fig. 2. The two considered situations are depicted on Fig. 1 by triangle combinations numbered 1 and 2 for the far term, while triangles numbered 1 and 3 are related to near term interaction. Using a combination of integration orders P and Q for source and observation triangles, respectively, ranging from $P = 1, \dots, 20$ and $Q = 1, \dots, 20$, the real and imaginary parts of the solution are presented independently.

The unit cube and the associated triangles are first scaled such that $a = \lambda/5$, $b = a/2$, where a is the length of cube side, and b is the length of triangle edge, while λ is the wavelength. Irrespective of radio frequency, in case of constant electrical length, i.e. $ka = const.$, both real and imaginary part of the solution converges similarly. As seen on Fig. 2a), obtained at 6 GHz, the increase of

integration points results in the convergence on both real and imaginary part of the solution. The same result can be depicted in a different manner, as shown on Fig. 2b), where the solution is represented on a (P, Q) square. The results obtained using increased number of integration points is denoted by moving from left to right for Q , and from top to bottom for P . In case when, going from top left to bottom right, the shade of grey becomes uniform, it means that the solution converges.

The checkered pattern, on the other hand, means that the convergence can not be guaranteed and further steps are in order. This can be illustrated on the results presented in lower row of Fig. 2. In case when purely numerical approach is used to solve the near triangle configuration, as seen on Fig. 2c), the real part of the solution behaves rather erratic at low integration orders. The convergence is obtained only in case when integration orders on both triangles are increased to 10-12. The very slow convergence of the solution (real part) is evident from the checkered pattern shown on Fig. 2d).

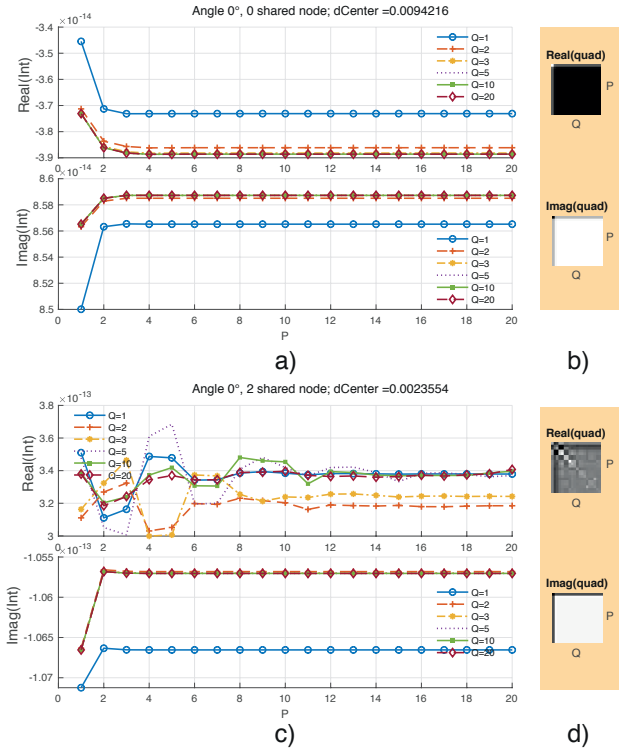


Fig. 2. Convergence of real and imaginary part of integral using several quadrature orders ($Q = 1, 2, 3, 5, 10, 20$). First row related to far combination of triangles, a), while second row is related to combination of near triangles sharing an edge, c). Visualization using a PQ -square, b) (far) and d) (near).

As the integral equation formulations lead to a fully populated matrices where the number of unknowns N is frequency related, the computational cost of such algorithm can become very expensive as the frequency increases. Thus, the following set of results are related to two frequencies related to 5th generation of mobile communications (5G) frequency spectrum utilized in Croatia,

i.e. that of 0.7 GHz and 3.6 GHz. To investigate the effects of triangle size, the results are obtained without scaling the geometry of unit cube.

The convergence results for two triangle combinations, including far and near interaction, are presented on Figs. 3 and 4, respectively, using (P, Q) squares to illustrate the behaviour of increasing the integration order.

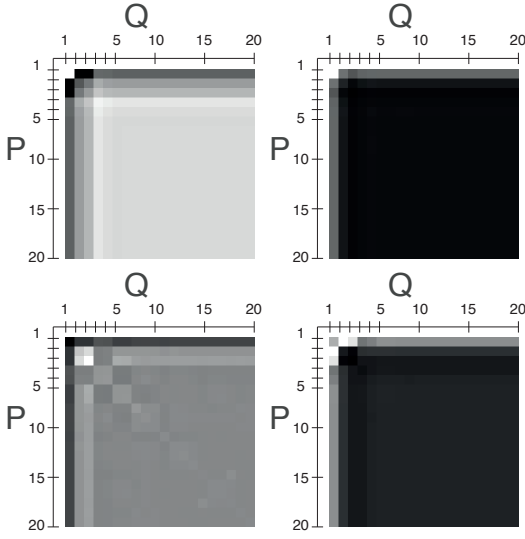


Fig. 3. P, Q -convergence test for far (first row) and near (second row) triangle combinations. Real part of the solution (left column) and imaginary part of the solution (right column) are showed with respect to increasing integration order P for inner and Q for outer triangle, respectively. Obtained at 0.7 GHz. Notice the checkered pattern in case of near interaction.

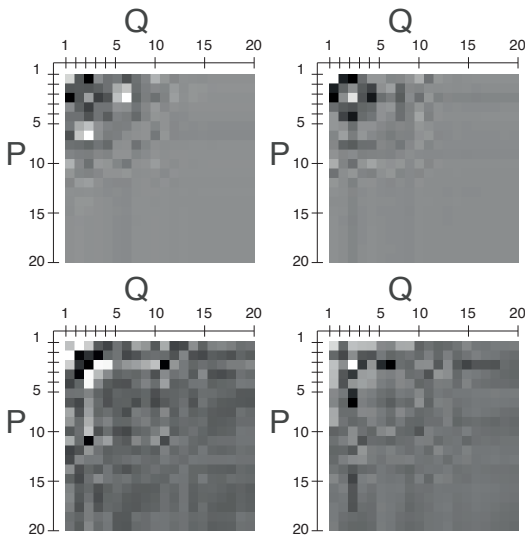


Fig. 4. P, Q -convergence test for far (first row) and near (second row) triangle combinations. Real part of the solution (left column) and imaginary part of the solution (right column) are showed with respect to increasing integration order P for inner and Q for outer triangle, respectively. Obtained at 3.6 GHz. In both cases the checkered pattern occurs.

As illustrated on Fig. 3, the results obtained at 0.7 GHz show that, in case of near triangle interaction (triangles sharing an edge), it is necessary to utilize higher integration order to ensure the convergence on the real part. On the other hand, at frequency of 3.6 GHz, i.e. when the triangle size compared to wavelength is not adequately small, as results on Fig. 4 show, in case of near interaction, even the utilization of highest integration rules does not guarantee the convergence. This shows that more finer discretization of the problem geometry should be utilized. Furthermore, if the utilized discretization is not fine enough, even in case of the far interaction, the checkered pattern occurs when lower integration rules are used. Thus, to ensure the convergence, it is necessary to use integration with higher number of points, resulting in the increased computational cost and longer processing time.

Finally, the question of selecting an optimal P and Q integration orders should be addressed. The unit cube and the associated triangles are scaled by half in several iteration steps ($n = 1, \dots, 8$). The discretization steps numbered $n = 4, 5, 6, 7, 8$ correspond to discretization schemes denoted as: 1/8, 1/16, 1/32, 1/64, and 1/128, respectively.

As an example, the number of integration points of integration order $(P, Q) = (7, 7)$ compared with lower integration orders at several discretization schemes (1/8 - green, 1/16 - purple, 1/32 - red, 1/64 - blue, 1/128 - yellow), is showed on Fig. 5.

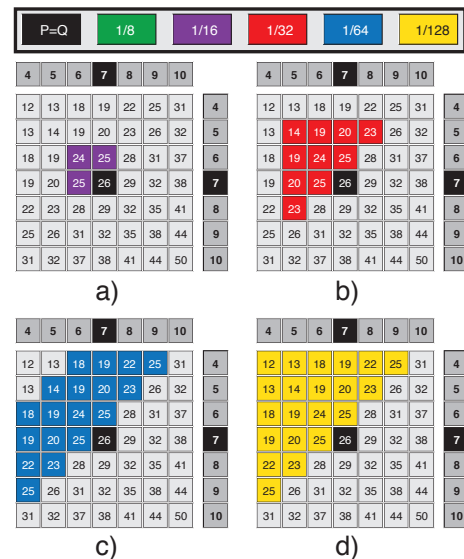


Fig. 5. Comparison of $(P, Q) = (7, 7)$ with lower integration orders with respect to discretization scheme: a) 1/16 - purple, b) 1/32 - red, c) 1/64 - blue, d) 1/128 - yellow. All coloured fields denote lower relative error compared to $(P, Q) = (7, 7)$.

Each field from the square denotes the total number of integration points used for both inner and outer triangles.

So, for example, at integration order $P=7$, 13 integration points are used per triangle, hence, 26 points in total. For each (P, Q) combination, the relative error with respect to reference value is determined using:

$$\text{Relative error} = \frac{|I_{\text{quad.}} - I_{\text{ref.}}|}{|I_{\text{ref.}}|} \quad (4)$$

where $I_{\text{quad.}}$ denotes the value at particular integration order (P, Q) , and $I_{\text{ref.}}$ is the reference value selected as the highest integration order, i.e. $P = 20, Q = 20$.

All the coloured fields, at the respective discretization scheme, denote the integration order with lower relative error compared to considered $(P, Q) = (7, 7)$ order.

The results show that at each discretization scheme, lower integration rules with lower number of integration points could be used. For example, at discretization level 1/32, shown on Fig. 5b), all the red coloured fields denote integration orders with lower relative error compared to $(P, Q) = (7, 7)$. Hence, the number of integration points in this case could be almost halved. These results suggest that, as the lower integration order could be utilized, depending on the discretization scheme, the time required for filling system matrix could be effectively reduced without necessarily sacrificing the solution accuracy.

Finally, as an illustrative example of EFIE implementation, the results for the electric and magnetic current densities \vec{J} and \vec{M} are shown on Fig. 6. The spherical lossy dielectric object is illuminated from above by a horizontally polarized plane wave. Several examples of application of EFIE include problems such as electromagnetic-thermal dosimetry [9], transcranial magnetic stimulation [10], as well as stochastic dosimetry of the human brain [11]. More details on the particular application can be found in [9], [10], [11].

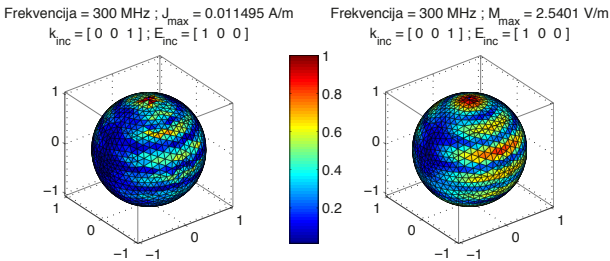


Fig. 6. Illustrative results obtained using EFIE formulation. Equivalent electric current \vec{J} and magnetic current \vec{M} , respectively, on the spherical surface S due to vertically incident, horizontally polarized plane wave.

IV. CONCLUSION

The paper presented a rather simple and effective approach for selecting an optimal numerical integration rule in terms of lowest number of integration points. Numerical example included one of the double surface integrals occurring in numerical implementation of electric field

integral equation formulation. The examples are considered at several 5G frequencies utilized in Croatia. It was demonstrated that a simple (P, Q) -test can facilitate an illustrative way showing whether convergence will occur when higher integration rules are used and can also indicate the situations when the increase of integration points will not necessarily result in the convergence. Further investigation showed that depending on the discretization scheme used, the matrix fill time could be lowered by using selected lower integration orders without losing the solution accuracy.

REFERENCES

- [1] M. Cvetković and D. Poljak, 2014, September. *An efficient integral equation based dosimetry model of the human brain*. In IEEE International Symposium on Electromagnetic Compatibility, 2014, 375-380.
- [2] M. Cvetković, D. Poljak, A. Lojić Kapetanović, and H. Dodig, *Unit cube test for double surface integrals in frequency domain integral equation formulations*, submitted to 5th International Conference on Smart and Sustainable Technologies (SpliTech 2021).
- [3] M. Cvetković and D. Poljak, "Electromagnetic dosimetry based on EFIE formulation and RWG basis function," Boundary Elements and other Mesh Reduction Methods XLI, vol. 122, (2019), 143-152.
- [4] Rao, Sadasiva, et al. "Electromagnetic scattering by surfaces of arbitrary shape." IEEE Trans. Antennas Propag. 30, no. 3, 1982, 409-418.
- [5] Dunavant, D. A. "High degree efficient symmetrical Gaussian quadrature rules for the triangle." International Journal for Numerical Methods in Engineering 21, no. 6, 1985: 1129-1148.
- [6] Wandzurat, S. and Xiao, H., "Symmetric quadrature rules on a triangle. Computers & Mathematics with Applications, 45(12), 2003, 1829-1840.
- [7] Savage, J.S. and Peterson, A.F., "Quadrature rules for numerical integration over triangles and tetrahedra. IEEE Antennas and Propagation Magazine, 38(3), 1996, 100-102.
- [8] M. Cvetković, et al., *Unit cube test for double surface integrals in frequency domain integral equation formulations*, submitted to 5th International Conference on Smart and Sustainable Technologies (SpliTech 2021).
- [9] Cvetković, M. and Poljak, D., *Electromagnetic-thermal dosimetry comparison of the homogeneous adult and child brain models based on the SIE approach*. Journal of Electromagnetic Waves and Applications, 29(17), 2015, 2365-2379.
- [10] Cvetković, et al., *Transcranial magnetic stimulation induced fields in different brain models*. Journal of Electromagnetic Waves and Applications, 30(14), 2016, 1820-1835.
- [11] Cvetković, et al., *Stochastic Sensitivity in Homogeneous Electromagnetic-Thermal Dosimetry Model of Human Brain*. Applied Computational Electromagnetics Society Journal, 31(6), 2016.